Hydrogenated defective graphene as an anode material for sodium and calcium ion batteries: a density functional theory study

Amir H. Farokh Niaei[a], Tanveer Hussain[a], Marlies Hankel[a] and Debra J. Searles[a,b*]

[a] Centre for Theoretical and Computational Molecular Science, Australian Institute for Bioengineering and Nanotechnology, The University of Queensland, Brisbane, QLD, 4072, Australia

[b]School of Chemistry and Molecular Biosciences, The University of Queensland, Brisbane, QLD, 4072, Australia

Abstract

Recent experimental studies indicated that hydrogenation improves the performance of graphitic materials used as anodes in lithium and sodium ion rechargeable batteries. Here, results of density functional theory calculations are presented to demonstrate that this is also effective for both sodium and calcium ion batteries. It is shown that this can be explained by the increase in binding strength of the metal adatom to the hydrogenated graphene, compared to its binding to graphene and also an increase in the inter-layer spacing of the layered materials. According to our calculations, whereas Na and Ca bind weakly to the graphene sheet with binding energies of -0.763 and -0.817 eV, they bind more strongly to the single layer of the proposed hydrogenated graphene sheet ($C_{68}H_4$) with binding energies of -1.670 and -2.756 eV, respectively. Furthermore, although Na does not intercalate strongly in the layers of the $C_{68}H_4$ material, up to 16 Ca can intercalate into the bulk layers of this material giving an electrical capacity of 591.2 mAh/g and a 29.3% expansion of the inter-layer distance. Thus, hydrogenated defective graphene provides an anode material that enhances the performance of rechargeable batteries compared to graphene, using metals that are cheaper than lithium.

* Corresponding author. Tel: +61 7 3346 3939
Email: d.bernhardt@uq.edu.au

1. Introduction

Recently, investigations on the possibility of developing sodium (Na) and calcium (Ca) ion rechargeable batteries have become more widespread. Since 2000, when Stevens and Dahn [1] inserted sodium into hard carbon materials, much of theoretical and experimental work has been carried out to see if efficient Na ion batteries (NIB) and Ca ion batteries (CIB) can be realised through the selection of appropriate electrode materials [2-6]. The electrode materials that have been considered include a variety of two-dimensional carbon materials and non-carbon materials [4, 6]. Since Na/Ca are more abundant than lithium, NIBs and CIBs are cheaper, and therefore favourable alternatives to lithium ion batteries (LIBs). In addition, Ca has the advantage that its ion has a +2 charge compared with +1 for Li and Na [7-9], although its atomic mass is higher.

Graphite has been most widely used as the anode material for LIBs [10, 11]; however, graphite does not bind Na and Ca atoms sufficiently strongly for Li to be replaced by them [12-14]. Moreover, graphite has an inter-layer distance of 3.35 Å and intercalation of Li is readily achieved, whereas intercalation of Na and Ca is not [15, 16]. This is because the atomic radii of Na (1.86 Å) and Ca atoms (1.97 Å) are significantly larger than Li (1.52 Å); 22% and 30% larger respectively [17]. Cao et al. [16] suggested that the minimum inter-layer distance required for Na intercalation would be 3.70 Å. In accordance with this, Komaba et al. [18] found that the inter-layer distance of the disordered carbon (or hard carbon) that they studied was 3.80 Å, made it possible for Na to intercalate. Another issue that prevents the development of NIBs using Na is that Na has been found to bind more weakly to graphene than other alkali metal and alkaline earth metal atoms. Liu et al. [12] found that the weak binding of Na (and Mg) on a graphene layer can be attributed to the relative magnitudes of ionization energy of the metal atoms and coupling between the graphene and the metal cations. Thus, two possible ways of designing electrodes for NIBs and CIBs based on layers of carbonaceous materials are to select materials where the binding of the metals to that material is stronger and the inter-layer spacing is larger than for graphite.

A solution that has been considered to address the issue of weak binding is the use of defective graphene, including graphene with Stone-Wales (SW) defects, mono-vacancies (MV) (graphene with a single C atom removed) and di-vacancies (DV) (graphene with two adjacent C atoms removed). These structures have been synthesised and considered for metal atom adsorption [19-24]. Figure 1 shows a schematic view of these defects in graphene.

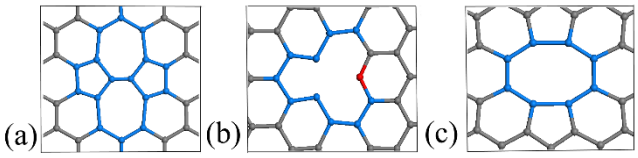

Figure 1. Optimized structures of graphene with (a) a Stone-Wales defect, (b) a mono-vacancy and (c) a di-vacancy. All atoms are carbon atoms. Blue atoms are those surrounding the vacancies or defects and the red atom in (b) indicates an under-coordinated carbon atom.

Vacancies in graphene layers can be produced by ion bombardment using ions such as Ar^+ at various energies [19, 20] with MVs and DVs, being the most likely defects formed after radiation of low energy beams over the graphene layer. Vacancies can also be produced from synthetic methods. For example, they can be formed from reduction of graphene oxide [25-27] or following an annealing process (thermal heating from 1000 to 1500 K), which can lead to very large defects [28]. Vacancies with odd numbers of C atoms removed have an under-coordinated carbon atom (commonly denoted to have a 'dangling bond' on the carbon atom), and introduces asymmetry in the configurations [21]. Moreover, the removal of a C atom results in a strain in the system, which can be partly compensated for by rearrangement of the structure in the vicinity of the vacancy. Due to the strain, C-C bond lengths around the vacancy can be longer than the normal C-C bond; for example, Carlsson and Scheffler observed bond lengths between 1.42 and 1.8 Å in defective graphene materials they considered [21]. Strain and dangling bonds can cause the carbon atoms in the vicinity of the vacancy to be more reactive than other C atoms in graphene.

There have been a number of studies that considered the effect of defects and vacancies (mainly SW, MVs and DVs) on the adsorption of Na or Ca with an aim to enhance the properties of electrodes for rechargeable batteries [29-31]. The theoretical electrical capacity of the anode material in mA h g^{-1} is:

$$E\ (mA\ h\ g^{-1}) = \frac{n_e\, n_M\, F}{3.6(n_M m_M + n_H\, m_H + n_C m_C)} \qquad (1)$$

where m_M, m_H and m_C are the atomic masses of the M, H and C atoms; n_M , n_H and n_C are the number of metal (M), hydrogen (H) and carbon (C) atoms in a unit cell and F is Faraday's constant, 9.648×10^4 C mol^{-1} . The value of n_e is given by the valency of the metal atoms (1 for Na and 2 for Ca). Considerable increase in the Na and Ca capacity has been observed on

defective graphene sheets compared to pristine sheets. For example, Datta et al. could obtain capacities of 646 mA h g^{-1} and 927 mA h g^{-1} for graphene sheets with DVs with a 25% defect rate [29] (note that in the paper of Datta et al., capacities of 1450 mA h g^{-1} and 2900 mA h g^{-1} are reported because the mass of Na and Ca are not included in the definition of the capacity, unlike in the current work where it is defined by equation (1)). Adsorption of Na or Ca was allowed on both sides of the sheet in that study. Tsai et al. found a loading of NaC_8 (225 mA h g^{-1}) could be obtained in a graphene bi-layer with an AA stacking and a DV on one of the layers, which resulted in the expansion of the inter-layer distance from 3.35 Å to 4.50 Å [30]. In a similar study, Yang et al. found that a loading of Na_6C_{35} (228 mA h g^{-1}) could be obtained in bi-layer graphene with an MV and an AA stacking [31]. In each of the studies mentioned above, Na or Ca accumulation near the vacancy or defect was observed.

Despite increased metal atom capacities, graphene layers with MVs are not expected to be suitable materials for batteries due to the dangling bonds on the carbon atoms, which make them quite reactive [32]. This could lead to bonding between layers and reduce the inter-layer distances. However, the under-coordinated C atoms can be hydrogenated to form more stable structures [33-36]. Casartelli et al. [36] applied density functional theory (DFT) to investigate the effect of the presence of C-H bonds on the structure of graphene by considering a hydrogenated MV. They considered 1 to 6 H atoms (2 for each carbon) on the three carbon atoms around a vacancy. They found that at 0 K, the fully hydrogenated system was most stable. However, due to entropic effects, at higher temperatures various degrees of hydrogenation could be achieved. Figure 2, shows the lowest energy structures for the MV with 1 or 2 H atoms.

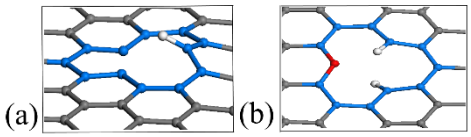

Figure 2: Side views of the most stable structure of (a) graphene with an MV and a single H atom, (b) graphene with an MV and two H atoms. The grey, blue and red atoms are C atoms, with those surrounding the vacancy coloured blue and the under-coordinated carbon atom coloured red. The white atom is a hydrogen atom.

According to Casartelli et al. [34], the creation of a C-H bond in the MV leads to a C-H bond directed out of the plane of the graphene sheet, as seen in Figure 2a. The carbon atom lies

0.694 Å above the graphene plane [34]. This is of interest as it indicates that hydrogenated MVs (H-MVs) may increase the inter-layer distance in layered bulk materials.

This possibility is consistent with experimental results of Yoon et al. [37]. They used a new synthetic route, using supercritical alcohol and which is referred to as a modified Hummers method, to fabricate hydrogen-enriched porous carbon nano-sheets (H-PCNs) with an H/C ratio of 2.3. The new material was then tested and found to be suitable for the anode of NIBs. The electrical capacity of the anode was 300 mA h g^{-1} at 50 mA g^{-1}, with a cycling stability of 2000 at 1-5 A g^{-1}. They suggested that the enhanced capacity could be attributed to the high number of hydrogen-terminated groups, a large number of defects on the sheets and the large inter-layer spacing of 3.8 Å between the material layers. Likewise, other researchers achieved a high electrical capacity using a hydrogenated carbonaceous material as anode materials for LIBs and NIBs [38-42], with the highest value for NIBs reported in these papers being 491 mA h g^{-1} [42].

In order to examine if hydrogenated defective graphene might be a useful material for Na and Ca ion battery electrodes due to strengthening binding energies compared to graphene and/or increasing inter-layer spacing in graphitic materials, we carried out a comprehensive study on a series of defective graphene sheets. Initial DFT calculations of the binding energies of Na on graphene sheets with vacancies and hydrogenated vacancies were carried out to determine which structures would be most likely to enhance alkali metal atom binding. We then examined the binding of multiple Na and Ca atoms on single layers of this structure and a model of the bulk, layered material. We expected similar enhanced binding for Ca as was observed for Na on the single layer. However, the different valency and similar size of the Ca atom suggested there could be an enhanced capacity with Ca. The Na and Ca binding energies and the expansion of the material with loading were determined to ascertain hydrogenated defective graphene could provide a suitable material for NIBs and CIBs. The results obtained should guide the selection of electrode materials for further experimental investigation.

2. Methodology

To study the interaction of Na and Ca on the hydrogenated defective graphene, DFT calculations were performed as implemented in the Vienna *ab initio* Simulation Package (VASP, ver. 5.3.5 and 5.4.4) [43]. The system is considered to be periodic in two dimensions for the single layer studies and periodic in three dimensions for bulk layer studies. A plane-

wave basis set was used. Within this package, the generalized gradient approximation (GGA) with projector-augmented wave (PAW) method was selected [44, 45]. The Gaussian smearing parameter was set to 0.05 eV. To account for the van der Waals interactions, the DFT-D3 method of Grimme [46, 47] was used. For calculations considering a single layer of graphene with a defect, the Brillouin zone was sampled with a 3 × 3 × 1 k-point mesh and the bulk layers were sampled with 3 × 3 × 2 k-point mesh, using the Monkhorst-Pack scheme. For the density of states (DOS) calculations, a 11 × 11 × 1 k-point grid of was used. The cut-off energy for the plane-wave basis set was selected to be 700 eV. The energy convergence criterion was selected to be 1×10^{-6} eV for most of the cases and 1×10^{-4} eV for the bulk cases. The force convergence criterion was selected to be between 0.05 eV $Å^{-1}$ and 0.01 eV $Å^{-1}$. The number of k-points and cut-off energy, force and energy convergence criteria were optimized in preliminary calculations [48]. Moreover, the cell sizes were optimized by cell size variation or using automatic cell size optimization in VASP for more complex bulk cases with a high number of atoms. Charges on the atoms were calculated using a Bader charge analysis [49, 50].

The binding energy between metal atoms and the substrate was determined by:

$$E_b = \frac{E(S.M_n) - n_M E(M) - E(S_o)}{n_M} \quad (2)$$

where $E(S.M_n)$ is the total energy of the substrate loaded with n_M metal atoms (Na or Ca), $E(M)$ is the energy of the metal M as an isolated atom, and $E(S_o)$ is the energy of the 2D substrate material in its optimal geometry. Using this definition, a negative binding energy indicates that the binding is energetically favourable.

In order to calculate the contribution of the binding energy due to the interaction between a group of adsorbed Na or Ca atoms and the substrate [51], we also define an 'interaction energy' as follows:

$$E_{int} = \frac{E(S.M_n) - E(M_n) - E(S_d)}{n_M} \quad (3)$$

where, $E(M_n)$ is the total energy of n metal atoms considered as an isolated group and $E(S_d)$ is the energy of the substrate only, in the configuration it adopted after adsorption of the metal adatoms (the deformed substrate). The value of $E(S_d)$ is higher than the value of $E(S_o)$, the substrate before metal adsorption. A negative value of E_{int} indicates a favourable interaction between groups of metal adatoms and the substrate [51].

3. Results and discussion

Graphene sheets with five different vacancies were considered in this work, and their optimised structures are shown in Figures 1b and c and Figure 3. They differ due to the number of C atoms removed and are referred to as a mono-vacancy graphene (MVG, Figure 1b), di-vacancy graphene (DVG, Figure 1c), tri-vacancy graphene (TVG, Figure 3a), quad-vacancy graphene (QVG, Figure 3b) and 24-vacancy graphene (24VG, Figure 3c) [32]. 24VG was selected as a representative large pore so see the effect of size on the results.

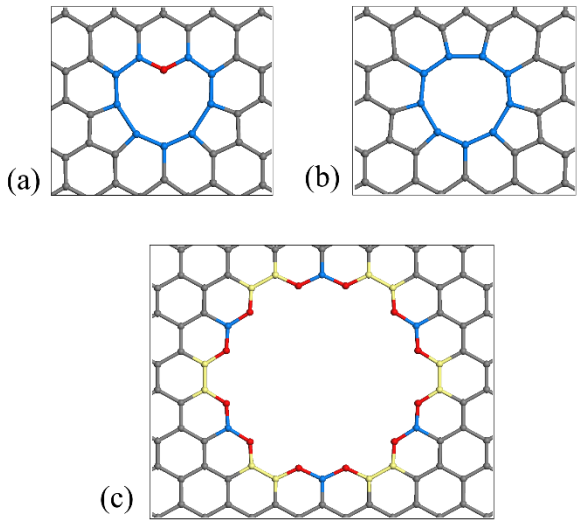

Figure 3: Top view of graphene with a (a) tri-vacancy, (b) quad-vacancy, and (c) 24-vacancy. All atoms are carbon atoms. Those coloured in red denote under-coordinated carbon atoms and those coloured in blue surround the vacancy. In (c) carbons involved in armchair type and zig-zag type edges around the vacancy are also distinguished by colouring in yellow and blue, respectively.

The presence of vacancies caused stress in the system, changes in the bonding of the C atoms, and changes in the cell size of the periodic structures in the defected sheets compared to that of pristine graphene. The optimised cell parameters are shown in Table 1 where we assumed $a=b$.

Table 1: The lattice vector lengths for graphene sheets with various vacancies

Material	Lattice vector lengths (a & b) / Å	% difference from graphene
Graphene	14.81	-
MVG	14.77	- 0.3 (contraction)
DVG	14.67	- 0.9 (contraction)
TVG	14.65	- 1.1 (contraction)
FVG	14.54	- 1.8 (contraction)
24VG	22.27	+ 0.3 (expansion)

Note the cell sizes for systems considered in Figures 3a and 3b are based on smaller supercells of the graphene sheets (14.81 Å) than that in Figure 3c which is based on a larger supercell with length 22.27 Å. According to the results shown in Table 1, there are small changes in the cell sizes induced by the vacancies.

3.1 Hydrogenated vacancies in graphene

Casartelli et al. [36] showed that hydrogenation of an MV by up to 6 H atoms formed energetically stable structures. Similarly, we considered various degrees of hydrogenation of the five defect models used here. The hydrogenation energy (ΔE_H) for the reaction:

$$C_nH_i + H \longrightarrow C_nH_{i+1} \qquad (4)$$

was calculated in the usual way:

$$\Delta E_H = E(C_nH_{i+1}) - E(C_nH_i) - E(H) \qquad (5)$$

where $E(C_nH_i)$ denotes the energy of the reactant, i = 0,1,… and $E(H)$ denotes the energy of the isolated H atom. The structures and formation energies for the hydrogenated MV are shown in Figure S1 and presented in Table S1, and the structures of selected hydrogenated DVG, TVG, QVG and 24VG structures are shown in Figure S2. Note that the notation used to refer to the different structures (e.g. H2-MVG) gives the number of hydrogen atoms after 'H' and the type of vacancy after the dash. It should be noted that H2-MVG has a carbon atom with a dangling bond on it, which is indicated in red in Figure S1b. The result of ΔE_H obtained for the hydrogenated MVs (Table S1) are in well accordance with those of Casartelli et al. [34, 36].

For the DVG, QVG and 24VG, various degrees of hydrogenation were considered. These structures are shown in Figure S2, and it is clear that for the smaller vacancy defects, the H atoms and some of the C atoms around the vacancy are out of the plane of graphene sheet. However, for H12-24VG the H and C atoms are in the plane, indicating the movement out of the plane was due to the proximity of other atoms. Once the pore size is increased to that of 24VG, there is sufficient space for the H atoms to become planar. This would limit the utility of hydrogenation in increasing the spacing between layered sheets, although the large pore itself might somewhat compensate for that, providing space to accommodate Na and Ca atoms. For TVG, there is a dangling bond on one carbon atom around the vacancy, so adding 1 H atom will saturate that. This structure is shown in Figure S2c, and it is clear that the H and C atoms are all in the plane of the graphene sheet; therefore, this structure might not increase the inter-layer spacing greatly. The hydrogenation energy of H1-TVG is -4.92 eV, which is higher than the ΔE_H of H1-MVG in absolute value (-4.25 eV).

3.2 Na adsorption on defective and hydrogenated defective graphene

The capabilities of the defective and hydrogenated graphene materials to adsorb (or bind) Na atoms over different sites were considered. For this study, Na was considered because it binds more weakly to graphene than Ca (-0.763 eV and -0.817 eV, respectively for a single metal atom on C_{72}). However, we expected that if enhancement was observed for Na, it would also be observed for Ca. Four different types of binding site are distinguished, as shown in Figure 4a. In Figure 4b, the binding energy of Na at each of these sites on a range of different materials is given, with the blue solid line indicating the cohesive binding energy of Na (-1.113 eV), and the black dashed line indicating the binding energy on pristine graphene (-0.763 eV). In addition, the binding energies of multiple Na atoms at their optimised positions is given to provide an indication of the maximum loading. The values of the binding energies are presented in Table S2.

According to Figure 4b, all graphene sheets with vacancies (MVG, DVG, TVG QVG and 24VG) bind Na strongly at sites A and B. The binding energies at sites C and D are also stronger than the cohesive energy and the binding energy of Na on pristine graphene. The binding at A and B was the strongest for systems with under-coordinated carbon atoms, and increased as the pore became larger. This behaviour is consistent with that demonstrated previously [29, 30, 32]. Our recent calculations for Na bound to graphdiyne showed similar behaviour, in that the Na preferred to bind in the large pores (-2.53 eV) than over the six-membered ring (-1.48 eV) [48]. For the material to be suitable as an electrode in rechargeable

batteries, the binding should not be too strong or the desorption of Na will be too difficult during the discharge process or for the material will distort, and not vary too much from site to site or mobility will be limited. In most cases, the binding at sites A and B is expected to be problematic due to these reasons.

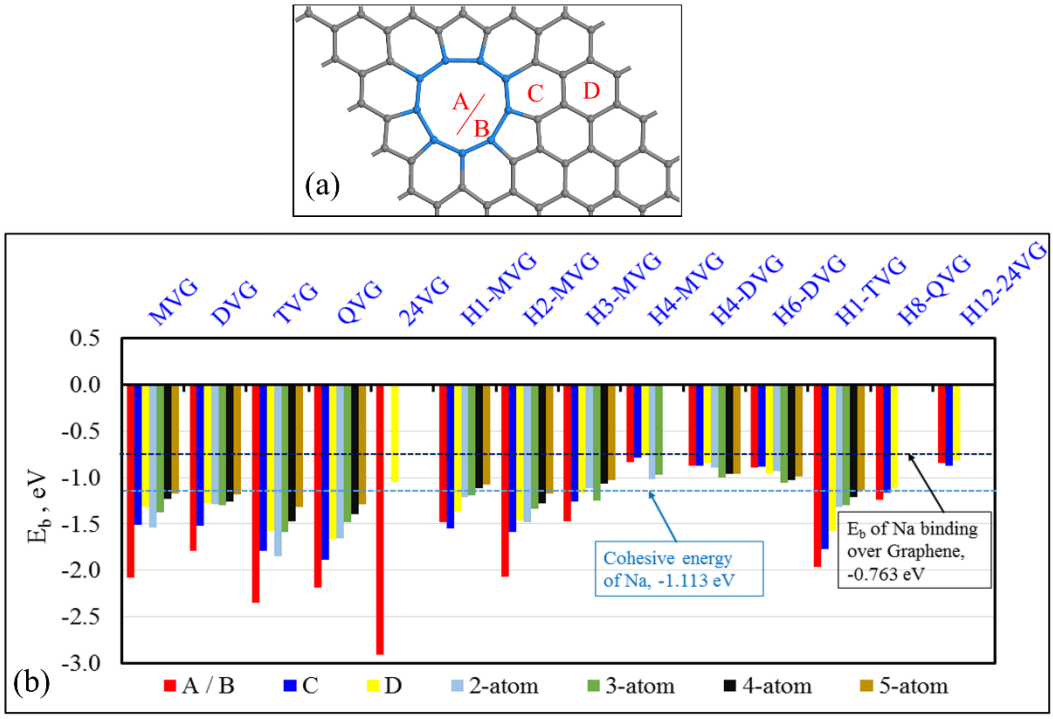

Figure 4 (a) Schematic diagram identifying the different positions for adsorption of Na in a graphene material with typical vacancies. Sites A (over the centre of a vacancy defect) and B (near the edge of a vacancy defect) generally represent the most stable sites over the defect. Sites C and D are the first and second most stable ring away from the vacancy, respectively. (b) A bar chart showing the E_b of Na at the various sites shown in (a) and for 2, 3, 4 and 5 Na atoms in their minimum energy positions over and around the vacancy including the rings nearby. If there is no coloured bar seen for a material and its site, it means that Na was not able to be adsorbed at that site. For 24VG and H12-24VG we did not consider 2 and more Na adatoms.

In contrast to the materials with vacancies, the hydrogenated defective materials in the bar chart show varied results for adsorption of a single Na atom. The materials H1-MVG, H2-MVG, H3-MVG and H1-TVG had E_b values that are stronger than the cohesive energy of Na

[13]. Although most other materials bound Na more strongly than graphene, in some cases the magnitude of E_b was less than the Na cohesive energy, which could lead to the clustering of the atoms if more than one Na atom was available. For example, cases with higher number of H atoms in the vacancy resulted in weaker binding as shown in Figure 4b, which shows the effect of the number of hydrogen atoms on the binding energies. However, this is not the case for H2-MVG, which of all the hydrogenated materials binds Na most strongly. This is due to the third carbon atom around the vacancy having a dangling bond and which is not saturated with hydrogen as shown in Figure 1b and Figure S1b. H2-MVG is expected to be difficult to produce experimentally due to is reactivity and because it is less stable than other materials [36]. However the other materials have Na binding energies at sites A/B that are approximately 0.1 – 1.0 eV higher than the cohesive energy of Na, and are expected to be suitable materials for anode according to this constraint.

Another point to note is that four graphene materials with vacancies (MVG, DVG, TVG and QVG), H2-MVG and H1-TVG can all bind up to at least 5 Na atoms over the vacancy or around it (*i.e.*, the average binding energy is less than the cohesive binding energy). Moreover, H1-MVG and H3-MVG bind 3 adatoms (see Table S2). This indicates that these materials could be of interest for NIB electrode materials. Figure 5 depicts the positions of the 5 Na adatoms on the defective and hydrogenated defective graphene sheets for structures where the binding energy per Na atom was stronger than the cohesive binding energy of Na, or close to it. According to Figure 4b, even when Na atoms are away from the vacancy and over the hexagonal rings, the average magnitude of the E_b values are larger than the cohesive energy of Na (in Figure 4a, sites C and D, blue and yellow bars). This is consistent with the results of Tsai et al. [30] and Yang et al. [31].

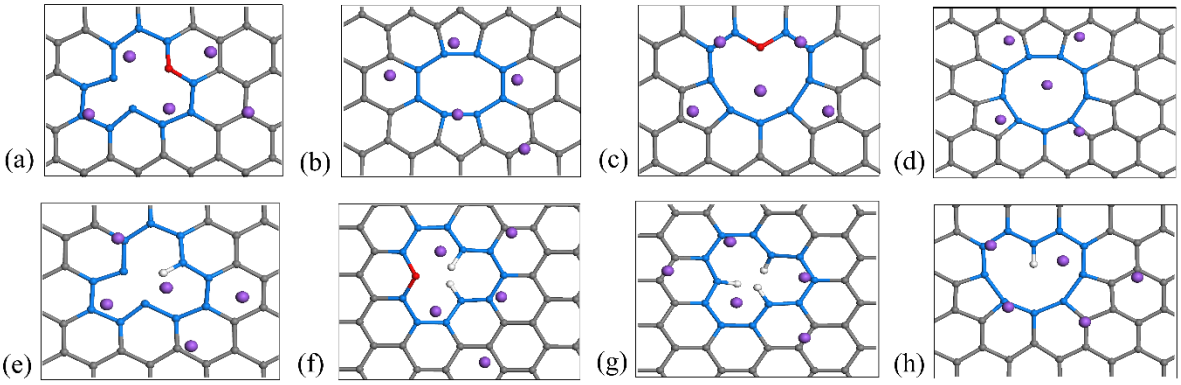

Figure 5. The position of 5 Na adatoms on various materials: (a) MVG, (b) DVG, (c) TVG, (d) QVG, (e) H1-MVG, (f) H2-MVG, (g) H3-MVG and (h) H1-TVG. The white atoms are hydrogen atoms, the purple atoms are Na atoms and all others are C atoms. The red atoms in (a), (c) and (f) indicate a carbon atom with a dangling bond and the blue atoms are those surrounding a vacancy.

3.3 Na adsorption on large pores of 24VG sheets

As already discussed, Na binds strongly to the 24VG sheet, but not to the H12-24VG sheet, which is consistent with the result of Okamato [32] for the Li adsorption on the similar defective graphene. However, in both cases, there are different sites at which the Na can bind, and it is of interest to consider the relative binding energies at several different sites in/near the pores. Figure 6 shows the sites considered on each of the two materials and Table 2 summarises the values of E_b for those sites.

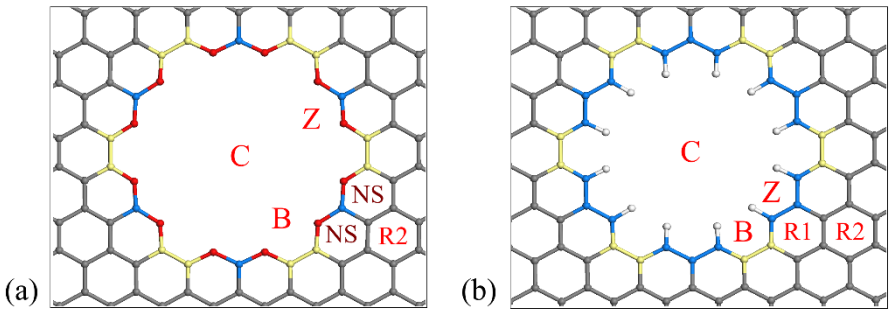

Figure 6 (a) Structure of 24VG, with possible adsorption sites labelled. Site C is at the centre of the vacancy, site Z is adjacent to the zig-zag type edge, and site B is adjacent to the armchair type edge. NS denotes sites where adsorption does not occur, and atoms initially placed there will move to site B. (b) Structure of H12-24VG with the possible adsorption sites labelled (C, Z, and B). Sites R1 and R2 are the two rings away from the vacancy. Armchair type and zig-zag type carbons around the vacancy are also distinguished by colouring in yellow and blue, respectively. Red coloured carbon atoms are those with a dangling bond.

Table 2. The binding energy of Na and its distance from the 24VG and H12-24VG materials for various sites

Sites defined in Figure 6	24VG		H12-24VG	
	E_b / eV	h_{ad} / Å	E_b / eV	h_{ad} / Å
C	-0.968	0.0	-0.249	0.0
B (Armchair)	-2.909	0.69	-0.842	2.18
Z (Zig-Zag)	-2.706	0.0	-0.724	2.25
R1	NS[a]	-	-0.871	2.20
R2	-1.043	2.23	-0.817	2.20

[a] NS denotes that Na does not stably bind at this site

From Figure 6a and the binding energies in Table 2 we see that that the strongest binding is at site B (in front of the armchair type edge within the pore). Site Z (in front of zig-zag type edge within the pore) is the second most stable site, and this is consistent with Okamato's result for lithium adsorption [32]. The sites indicated by NS in Figure 8a do not bind Na, and if initially we put Na at these sites, they move to sites B or Z on geometry optimization. Further from the pore at R2, the value of E_b is -1.043 eV. This is still stronger than the binding of Na to graphene, but weaker than the cohesive energy of Na. The high value of the binding energy at sites B and Z can be directly attributed to the existence of 12 dangling bond carbon atoms around the vacancy edge. By contrast, when we hydrogenate the 24VG to get H12-24VG, as seen in Figure 6b and Table 2, the E_b values decrease greatly to values that are too weak to prevent clustering. These results indicate that neither the non-hydrogenated nor hydrogenated 24VG sheets are suitable for battery materials: 24VG has many dangling bond carbon atoms which is likely to lead to binding with other sheets (although it strongly binds Na); and H12-24VG does not bind Na sufficiently strong. However, it is interesting to observe that the position at which Na binds most strongly is in the pore for 24VG but over the defective graphene surface for H12-24VG. In summary, the above results show that large pores within graphene will not enhance Na binding when it is passivated by hydrogen and will have problems associated with instability or reactivity if it is not passivated [32]. Therefore, we focus on the small vacancies in the following sections.

3.4 Na adsorption on single layer and bulk graphene with MV and DVs

Due to the fairly strong binding of Na to a H1-MVG evident from Figure 4b, it is of interest to examine how the binding energies of Na vary on sheets containing several MVs and the

maximum number of atoms that could be expected to be adsorbed. We firstly optimized a defective graphene sheet with 4 MVs in a 6x6 graphene supercell (C_{68} which we refer to as 4MVG), as shown in Figure 7a. This structure has a 5.55% defect concentration with respect to graphene, and adding more defects in the supercell was found to disrupt the structure of the layer. The geometrically optimized 4MVG structure (Figure 7a) is planar due to the triplet electronic state [34].

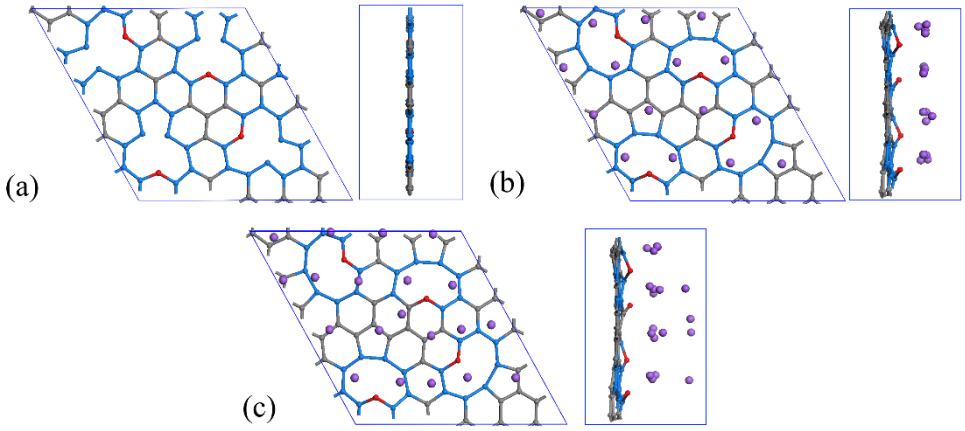

Figure 7. Top and side view of the optimized structure of (a) graphene sheet with 4 mono-vacancies (4MVG) (b) 16 Na atoms adsorbing on the 4MVG material (c) 20 Na atoms adsorbing on the 4MVG material, 4 of which forming a second layer on top of the first layer. Blue colours are those surrounding vacancies, red atoms are those with a dangling bond, and purple atoms are Na atoms.

In order to evaluate the ability of this structure to adsorb Na atoms, we optimised several initial configurations and found that a maximum of 16 Na atoms can bind to the 4MVG sheet in a single layer. The average E_b is -1.369 eV (stronger than the cohesive energy of Na), and the average height of adsorption (h_{av}) is 2.48 Å. The top and side views of the material with this loading are shown in Figure 7b. Examination of the top view in Figure 7b indicates that a fairly regular network of Na atoms is situated above the material, with the Na-Na distances varying between 3.5 and 4.2 Å. This is similar to the distances between the closest Na atoms in a single layer of Na arranged in the structure corresponding to that of the 110 surface of the bulk metal (Figure S3a) (3.54 – 3.64 Å). On addition of more Na atoms, the atoms start to form a second layer further from the sheet as shown in Figure 7c.

To test the intercalation of Na atom within the bulk layers of 4MVG, we optimized the structure with an AA stacking. This AA stacking was the most stable of the possible stackings considered and results in overlaying the two mono-vacancies in adjacent layers. The average inter-layer distance of this stacking is 3.37 Å, which is very similar to the inter-layer distance of graphene (3.35 Å [16]). Therefore, as expected, the vacancy defect does not result in a significant increase in the inter-layer distance. Moreover, this distance is smaller than the values of 3.70 Å reported by Cao et al. [16] and 3.94 Å reported by Tsai et al. [30] as the distance required for Na intercalation. Therefore, intercalation of Na within the 4MVG with AA stacking is likely to be difficult.

Figure 8a depicts top and side views of the 4MVG bulk layers intercalated with 1 Na atom over the mono-vacancy in AA stacking. The under-coordinated carbon atoms of the two adjacent MVs moved out of their planes and formed a bond of length 1.37 Å, which is very similar value to a carbon-carbon double bond length of 1.33 Å [17]. This is a shortcoming of the 4MVG material, because it causes a decrease in inter-layer distance of the 4MVG bulk layers to 3.32 Å. It also keeps the layers in fixed positions relative to each other and prevents them from sliding as normally seen in graphene stacking types (AB, ABA, ABC) [53]. These problems indicate that graphene sheets with a mono vacancy would not be suitable for use as materials for NIBs.

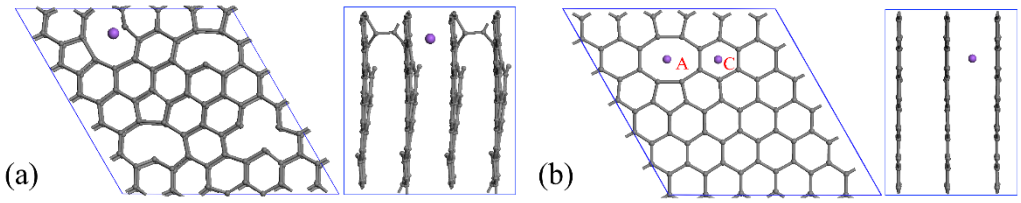

Figure 8 (a) Top and side view of the structure formed from geometry optimization of 4MVG bulk layers intercalated with a Na atom (purple). This results in bonding between the layers as shown in the right panel, with a carbon-carbon bond length of 1.37 Å. (b) Top and side view of the structure formed from geometry optimization of DVG bulk layers with an AA stacking intercalated with a Na at sites A or C. In the side views the Na atoms at the A and C sites are eclipsed.

We also inserted a Na atom between the layers of DVG with an AA stacking, which was the optimal stacking for the bulk layers. Even though Na bound strongly at both sites A and C

(defined in Figure 4) of a single layer DVG material (E_b values of -1.79 and -1.52 eV, respectively), in the bulk material these values are reduced to -1.74 and -0.71 eV, respectively. A large difference of 0.81 eV in the binding energy at site C in the bulk system indicates that Na atoms would bind strongly in the centre of the defect but weakly at site C, which means that this material is unlikely to be a suitable option for anode material since diffusion of the Na would be slow. Suitable bulk layers must provide strong binding energy at all the sites including the sites near the defects for a number of adatoms to intercalate.

3.5 Na and Ca binding on H-MVG single and bulk layers

Of the hydrogenated MVGs considered above, only the H1-MVG and H2-MVG materials bound Na strongly at locations near the MV. Indeed, H2-MVG has a dangling bond on the vacant carbon atom around the vacancy, as shown in red in Figure 2b. Therefore, C-C binding as shown in Figure 8a may occur for this structure. The optimized structure for H1-MVG is shown in Figure 2a, and it is found that the C-H bond length is 1.077 Å. In contrast to the planar MVG structure, the C atom in H1-MVG is 0.748 Å above the plane. By hydrogenating the 4MVG material (Figure 7a) with one hydrogen atom at each MV, $C_{68}H_4$, denoted by 4(H1-MVG), is obtained as seen in Figure 9a. Different structures can be formed with different combinations of direction of the C-H bond such as those shown in Figure 9. The structure in Figure 9a has all the H atoms on the same side of the sheet, which we refer to as cis-4(H1-MVG), and that in Figure 9b has two on one side and two on the other side, and we refer to it as trans-4(H1-MVG).

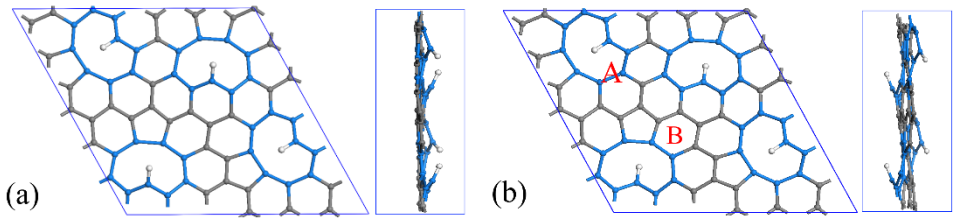

Figure 9. Top and side view of the 4(H1-MVG) sheet with (a) H atoms all on one side of the sheet and (b) half the H atoms on one side and half on the other. In (b) binding sites, A and B, are labelled. Blue colours are those carbon atoms surrounding vacancies, and white atoms are hydrogen.

The trans-4(H1-MVG) has a lower total energy than cis-4(H1-MVG), -628.50 eV versus -628.08 eV with 0.42 eV difference. Therefore, we selected trans-4(H1-MVG) for the rest of

our computations. Table 3 presents the binding energies of Na to trans-4(H1-MVG) at the two sites (A and B) indicated in Figure 9b. Initially we added 1 and 2 Na atoms to compare the binding energies at different sites. It is also of interest to compare the binding energy of Ca with that of Na, since Ca has two valence electrons (Na has one) and this is relevant to the electrical capacity (n_e = 2 in equation 2). In order to determine the maximum capacity of one side of the single layer, we have considered the binding energy of 12, 14 and 16 atoms on the same side. In addition, we considered the binding energy of 8, 10, 12, 14 and 16 atoms to each side of the sheet, (totally 16, 20, 24, 28 and 32 atoms, respectively). The results are presented in Table 3.

Table 3. Average binding energies and Bader charges for Na and Ca on trans-4(H1-MVG)

		Na		**Ca**	
Number of atoms and binding site		Average E_b atom / eV	Average Bader charge per atom / *e*	Average E_b atom / eV	Average Bader charge per atom / *e*
1 (@ A)	Binding to one side	-1.506	0.819	-2.115	1.352
1 (@ B)		-1.670	0.824	-2.756	1.336
2 (@ A & B)		-1.597	0.814	-2.376	1.005
12		-1.248	0.273	-2.137	0.507
14		-1.241	0.218	-2.103	0.493
16		-1.250	0.179	[a]	-
Max. capacity[b] / mA h g^{-1}		360.8 (16 Na)	-	547.0 (14 Ca)	-
16	Binding to both sides	-1.214	0.258	-1.960	0.607
20		-1.184	0.210	-2.008	0.582
24		-1.162	0.171	-2.074	0.550
28		-1.160	0.142	-2.063	0.531
32		-1.182	0.105	[a]	-
Max. capacity[b] / mA h g^{-1}		551.0 (32 Na)		780.4 (28 Ca)	

[a] In this case we were unable to bind a single layer of Ca atoms

[b] We define the maximum capacity as the point after which there might be sheet disruption (e.g. in the case of 16 Ca) or formation of another surface over the sheet (e.g. in the case of 20 Na)

Figure 10 depicts the top and side views of the single layer loaded with Na and Ca. According to the results of Table 3, all the magnitudes of E_b are lower than the cohesive binding energies of Na (-1.113 eV) and Ca (-1.840 eV) [13], and Ca has a stronger binding to the sheet. For both metal atoms, the preferred binding site is site B (see Figure 9). The average Bader charges [49, 50] on the metal atoms are higher for Ca (1.336 for a single atom at site B) than Na (0.824 for a single atom at site B) as expected from their valencies.

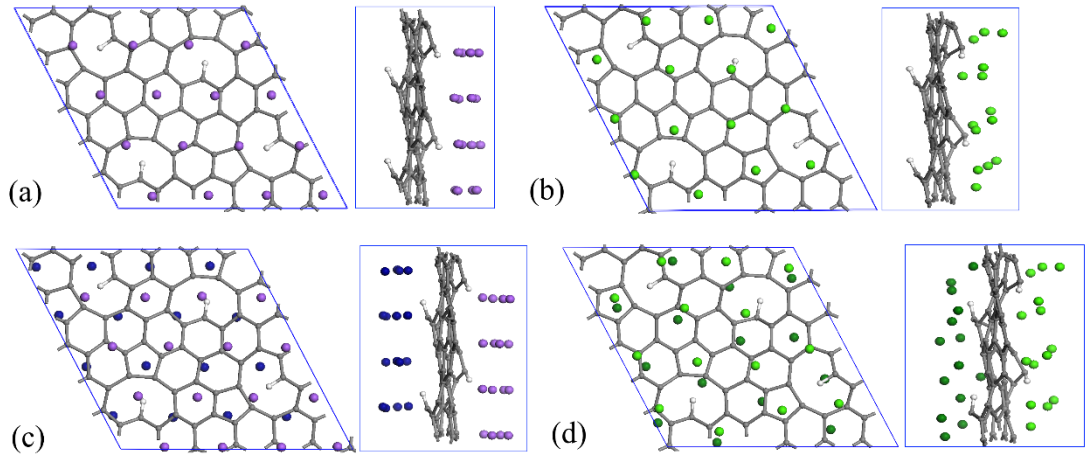

Figure 10: Top and side views of the trans-4(H1-MVG) with (a) 16 Na, (b) 14 Ca, (c) 32 Na, and (d) 28 Ca atoms. In (a) and (c) light and dark purple atoms are those Na atoms located over and behind the layer, respectively. In the same way in (b) and (d), light and dark green atoms are those Na atoms located over and behind the layer, respectively.

The distance between the Na-Na atoms in the case with 16 Na atoms on one side varies between 3.5 and 3.8 Å (Figure 10a). This is similar to the arrangement of the 16 Na atoms over the 4MVG sheet (see Figure 9b), and is also similar to the distance between two neighbouring Na atoms in a single layer of atoms arranged in the structure corresponding to the 110 surface of the bcc metal, 3.54 and 3.64 Å (Figure S3a). Similarly, for Ca adsorption (Figure 10b), the Ca-Ca distance varies between 3.5 and 5.1 Å, which is similar to the distance between Ca in a single layer of atoms arranged in the structure corresponding to the 100 surface of the fcc metal of 3.57 and 5.05 Å (Figure S3b). These similarities suggest that there is likely to be interactions between the Ca atoms.

We note that as the loading becomes high, the average charges on the metal atoms drop (see Table 3) which is in accordance with the previous result of Li on graphene [54]. Consideration of the charge distribution indicates that there is a general drop in charge for all the metal adatoms (e.g. with 16 Na atoms the charges range from 0.02 to -0.34 and with the 14 Ca atoms from -0.20 to -0.84). The same trends generally hold for the E_b of the adatom on the surface, except two cases: going from 14 to 16 Na adatoms on one side and from 28 to 32 Na adatom on the both sides. A small increase in the absolute value of E_b, the low values of the Bader charges on the atoms and the fact that the distances between the atoms are similar to that in the single atom metal sheets suggest that the interaction between the metal adatoms might be starting to dominate the behaviour, and that a metal surface is forming over the substrate. To get a better indication of the interaction between the metal adatoms and substrate, we have reported E_b, E_{int} (defined in equations 2 and 3) and E_f (the formation energy of the metal cluster from single isolated atoms) for Na and Ca, and the results are presented in Table 4.

Table 4: Values of E_{int} and E_f for Na and Ca adsorbed on the 4(H1-MVG) single layer material and comparison with E_f for the 2D metal surface.

Substrate + Adadtom	**Number of metal adatoms**	**E_b , eV/atom**	**E_{int} , eV atom**	**E_f, eV/atom**	**Energy of surface formation of pure metal atoms**
4(H1-MVG) single layer + Na	12 Na	-1.248	-0.987	-0.289	-0.894[a]
	14 Na	-1.241	-1.229	-0.037	
	16 Na	-1.250	-1.654	+0.385	
4(H1-MVG) single layer + Ca	8 Ca	-2.188	-1.420	-0.778	-1.024 [a]
	10 Ca	-2.137	-1.307	-0.910	
	12 Ca	-2.137	-1.200	-1.054	
	14 Ca	-2.103	-1.193	-1.061	

[a] Energy of metal surface formation in the Na 110 and Ca 100 configurations (Figures S1a and S1b)

As shown in Table 4, the values of E_f for the isolated clusters of Na or Ca atoms in the structures they formed on the substrate are mostly higher than the formation energy of Na and Ca atoms in ideal 110 and 100 configurations (Figures S1a and S1b), as expected. In addition, apart from the case where 16 Na atoms were adsorbed (in which the isolated Na structure was not stable), the E_{int} between the cluster and the substrate was lower in magnitude than E_b. This indicates that part of E_b was due to interactions between the metal atoms. The fact that the formation energy of the metal clusters is more positive than either E_b or E_{int} indicates that the metal atoms are interacting significantly with the substrate. This difference is larger for the smaller Ca clusters but the reverse trend is observed for Na; reflecting the fact that the isolated Na clusters become less stable as their size increases and the fact that their structure is highly affected by the strength of their interaction with the substrate.

3.6 The intercalation of Na and Ca in the 4(H1-MVG) bulk layers

In order to investigate the intercalation of Na and Ca within the bulk trans-4(H1-MVG) ($C_{68}H_4$) layered materials, we have carried out computations for 4 different types of stacking. The optimised structures of 4 different stackings are presented in Figure S4. It is found that the AA stacking has the lowest energy with an average inter-layer distance of 3.49 Å (separation of centre of mass of the carbon atoms in each layer), which is approximately 4% higher than the inter-layer distance in graphene and the AB2 stacking is least favourable with an energy that is 1.8 eV higher and an inter-layer distance 13.4% higher than that in graphene. We might not expect the distance to be much greater than that for graphene, due to the van der Waals forces between the layers [30, 55]. Comparing the energies of the 4 stackings (Figure S4), we observe that the lower energy, the smaller the inter-layer distance.

Selecting the AA stacking for the 4(H1-MVG) bulk layers, we calculated the Na and Ca intercalation energies, (see Table 5) while keeping the inter-layer distance fixed to be that of the minimum energy 4(H1-MVG) structure with no metal atoms. Figure 11 depicts the two sites in between the layers at which we placed Na or Ca adatoms. These were selected based on the results obtained for the monolayers. Site A is over the mono-vacancy and between the layers and site B is over a hexagonal ring close to the MV and between the layers.

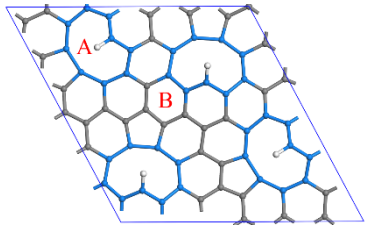

Figure 11: Location of sites A and B on 4(H1-MVG) bulk material with AA stacking type. In both cases, the Na or Ca atoms are located in between the layers. Blue atoms are those carbon atoms surrounding vacancies, white atoms are hydrogen all other atoms are carbon atoms.

Table 5: The E_b and Bader charge values for Na and Ca atoms at the sites A and B of the 4(H1-MVG) bulk layers

Atom	**Site A, E_b / eV**	**Site B, E_b / eV**	**Bader Analysis**	
			Charge on atom at Site A / *e*	**Charge on atom at Site B / *e***
Na	-0.649	-0.303	0.748	0.739
Ca	-2.793	-2.048	1.339	1.301

According to the results shown in Table 5, Na does not bind strongly between the bulk layers, with the E_b values being much weaker than the cohesive energy. As a result, clustering may occur when a number of Na atoms are intercalated between the layers. It was also found that the Bader charge values of Na is +0.75 *e* which is even lower than the Bader charge of 1 Na on a single layer of 4(H1-MVG) at 0.819 and 0.824 *e* (Table 3).

By contrast, Ca is found to bind strongly within the layers, with all the binding energies stronger than the cohesive energy of Ca (-1.840 eV). It is interesting to recall that both Na and Ca bound to the 4(H1-MVG) single layer, although Ca was still stronger. The binding energy of the Na is much weaker in the bulk system than on the single layer, whereas Ca is similar on single layers and in the bulk. Moreover, the amount of charge on the Ca when intercalated in the bulk 4(H1-MVG) (1.34 *e*) is very similar to that when it is on a single layer (1.35 *e*, see Table 3).

In order to investigate the effect of inter-layer distance of 4(H1-MVG) bulk layers on Na binding we considered the variation of E_b with expansion of the 4(H1-MVG) bulk layers intercalated with 1 Na atom on each layer at site A (Figure 11) (2 Na atoms in the supercell). This is similar to way that Tsai et al. [30] considered Na in bi-layers of graphene and defective graphene. The results are presented in Figure 12.

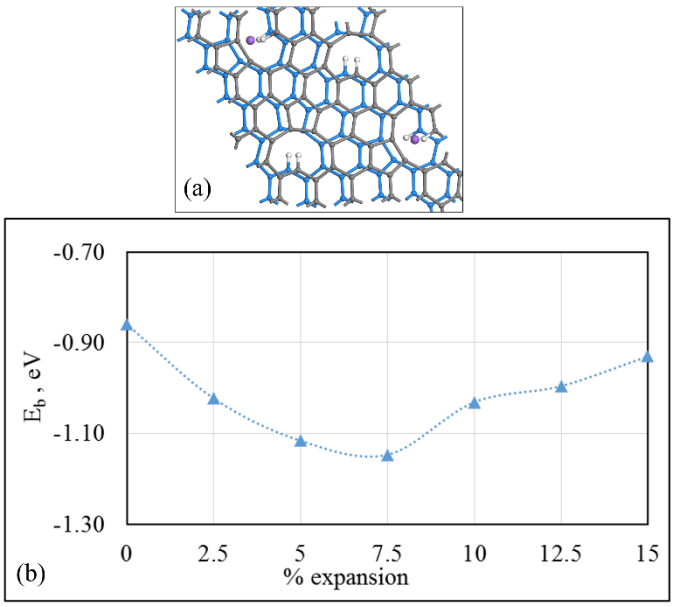

Figure 12: (a) Bulk 4(H1-MVG) intercalated with Na atoms (purple) at sites A. The white atoms are hydrogen and all others are carbons in the two different layers; (b) Variation of E_b for Na intercalated in 4(H1-MVG) bulk, with the % expansion of the inter-layer spacing compared to the material without Na.

From Figure 12b, we see that the minimum E_b occurred at approximately 7.5 % expansion of the layers compared to that of the material with no Na and the binding energy (-1.148 eV) is just a little stronger than the cohesive energy of Na. Therefore, expansion of layers does not improve the Na binding sufficiently to suggest that bulk 4(H1-MVG) would not be a useful material for NIBs. The expansion of the of 4(H1-MVG) bulk layers on intercalation of Ca is considered in the next section.

3.7 Loading 4(H1-MVG) bulk layered materials with multiple Ca atoms

In this section, we investigate the loading of 4(H1-MVG) bulk layers in a AA stacking with a number of Ca atoms in order to determine the maximum capacity and the expansion of the layers. We considered 2 to 32 Ca atoms in the supercell, with equal number of Ca atoms in each slit-pore. Figures 13a and b show the top and side views of the systems loaded with 2 and 32 Ca atoms. Figure 13c shows the variation of E_b values and expansion of the layers as a function of the number of Ca atoms that are intercalated.

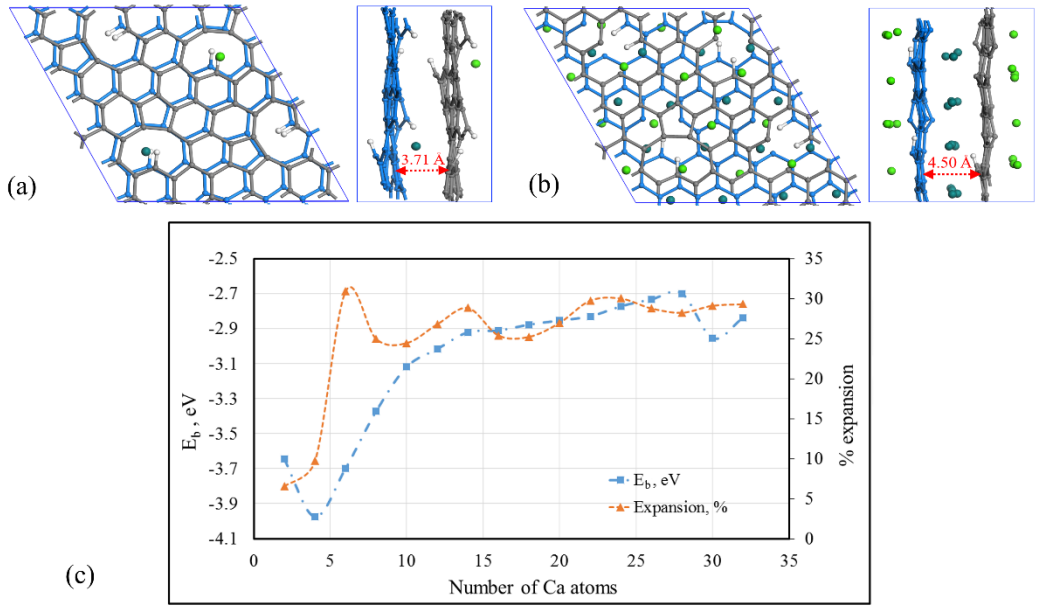

Figure 13: Binding energies per Ca atom for 4(H1-MVG) loaded with (a) 2 Ca atoms and (b) 32 Ca atoms. The H atoms are colored white, the Ca atoms are light or dark green depending on which slit pore they are located in, and the carbon atoms are gray or blue depending on the sheet they are in (c) Variation of the binding energy per atom, E_b, and expansion % of the bulk systems as a function of Ca loading.

From Figure 13, it can be seen that with 2 Ca atoms E_b is -3.65 eV and the bulk material has undergone a 6.6% expansion. With 32 Ca atoms E_b is -2.84 eV and expansion is 29.3%. Overall, the binding energy per atom becomes weaker with an increase in loading which is expected. The deviation of the behaviour from this trend is due to the symmetry of the system and/or the fact that there are many local minimum energy arrangements, and in some cases the global minimum might not have been found. The maximum value of expansion was found to be 31% with 6 Ca atoms, and it corresponds to the inter-layer distance of 4.56 Å. Similar expansion was observed in graphdiyne bulk layered materials loaded with 7 Na atoms on each layer ($C_{2.57}Na$) at 28% [48]. With more than 32 Ca atoms, we were unable to obtain a stable structure with a single layer of Ca atoms between the 4(H1-MVG) layers, so 32 was taken as the maximum loading. Furthermore, the Bader analysis shows that the average charge on a Ca atom with 32 Ca atoms is 1.17 *e* , which is higher than that obtained with 14 Ca atoms on one side of a single layer of 4(H1-MVG) (0.493 *e*) or 28 Ca atoms on both sides of the single layer (0.531 *e*) (see Table 4).

We note that intercalation of a relatively small number of Ca atoms results in expansion of the layers of 4(H1-MVG) and this expanded material allows other Ca atoms to intercalate. In addition, the existence of apical (non-planar) C-H bond in the basal defect (mono-vacancy) makes the inter-layer spacing sufficiently large to allow intercalation of the first Ca atom. Moreover, there is no disruption in the structure of the 2D material. According to this result and the definition above, the maximum capacity of 4(H1-MVG) bulk layers is 32 Ca atoms or $C_{68}H_4Ca_{16}$, equivalent to an electrical capacity of 591.2 mA h g^{-1}; this capacity is compatible with the electrical capacity of 300 mA h g^{-1} at 50 mA g^{-1} achieved by Yoon et al. for hydrogen enriched porous carbonaceous material [37] and 491 mA h g^{-1} achieved by Pramudita, et al. [42] for hydrogenated graphene (H-TEGO) selected for NIBs. Consequently, the combination of Ca with 4(H1-MVG) is predicted to be a promising anode material for CIBs.

3.8 Electronic Properties Density of States (DOS)

In this section, we briefly report the electronic properties of the studied systems through total (TDOS), partial density of states (PDOS) and charge density. Figure S5 depict the TDOS and PDOS for 4(H1-MVG) substrate, and 4(H1-MVG) + 1 Na and 1 Ca atoms. A single layer of 4(H1-MVG) is considered.

According to the TDOS in Figure S5a, there is no band gap, so the 4(H1-MVG) sheet is conductive as desirable for an anode material. The same holds for the two indicated carbon atoms as indicated in Figure S5b. Likewise, Figures S5c and d indicate that the there is no band gap for 4(H1-MVG) intercalated with 1 Na or 1 Ca atom. In addition, Figure S5e depicts the PDOS of the Ca and also the indicated carbon atom (red colour). According to this figure there is an overlap of the Ca states (blue curve) over the C states (yellow curve), which suggests bonding between the Ca atom and the indicated carbon atoms.

Charge densities for the 4(H1-MVG) with Na and Ca atoms adsorbed were also determined. The charge density difference is given by,

$$\Delta\rho = \rho_{4(\text{H1-MVG}) + \text{Na / Ca}} - \rho_{4(\text{H1-MVG})} - \rho_{\text{Na / Ca}} \quad (5)$$

where ρ is the charge density of the systems specified (*e Bohr*$^{-3}$). The charge density differences for the systems with single Na or Ca are shown in Figures 14a and b, with the blue colour indicating greater electron density on the carbon atoms and the red colour indicates positive charge around the Na or Ca cations. Regarding Figures 14c and d, there is also a considerable charge transfer from the 16 Na and 14 Ca atoms to the substrate. In this

case, the positive charge is delocalized among the Na and Ca, suggesting that the layer is becoming metallic. The system with 14 Ca atoms (Figure 14d) has more charge transfer (seen as a greater region of blue in Figure 14d). This is consistent with the higher valency for Ca than Na.

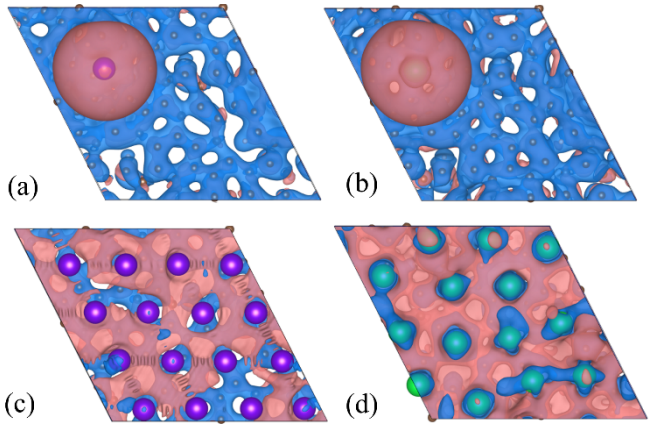

Figure 14: Charge density difference, the red and blue colours indicate regions where the charge becomes more positive or more negative, respectively, compared to the isolated metal atoms or substrate. a) 4(H1-MVG) + 1 Na, $\Delta\rho$ =0.0001 *e Bohr*$^{-3}$, b) 4(H1-MVG) + 1 Ca, $\Delta\rho$ =0.0001 *e Bohr*$^{-3}$, c) 4(H1-MVG) + 16 Na, $\Delta\rho$ =0.0007 *e Bohr*$^{-3}$, and d) 4(H1-MVG) + 14 Ca, $\Delta\rho$ =0.0007 *e Bohr*$^{-3}$. In c) and d), purple spheres are Na atoms and green spheres are Ca atoms, respectively.

4. Conclusion

The effect of vacancies on the binding of Na and Ca atoms to a variety of defective carbon-based 2D sheets have been considered. If defects result in under-coordinated carbons, the binding of the metal atoms is enhanced, but these materials are likely to result in linking of the layers and therefore saturation of the defects by hydrogenation is considered. The hydrogenated mono-vacancy or 4(H1-MVG) ($C_{68}H_4$) has apical C-H bonds at the basal plane. This results in an increase in the spacing between layers compared with graphite as well as enhancement in the binding of Na and Ca to the materials. However, only Ca provides sufficiently strong binding to the bulk layers of 4(H1-MVG) to prevent cohesion of the metal atoms. The bulk material provides a maximum capacity of 16 Ca within each AA stacked layer. This is equivalent to $C_{68}H_4Ca_{16}$ and 591.2 mA h g^{-1} electrical capacity which is comparable with experimental results for hydrogenated graphene [37, 42], which found that such materials could be useful as anodes for rechargeable batteries. The expansion of the stacked layers after Ca intercalation varies from 6.6% to 31.0%. These calculations

demonstrate that the enhanced performance of hydrogenated anode materials compared to pristine graphene [12, 13] could be both because of the stronger binding of the metal atoms to the substrate and the expansion of the material due to the apical C-H bond that acts as a side arm to expand the layers and enable intercalation. It also proposed that synthesis of structures similar to 4(H1-MVG) could be beneficial for battery materials.

Acknowledgements

The authors thank the Australian Research Council for support of this project through the LIEF program. This research was undertaken with the assistance of resources provided at the NCI National Facility systems at the Australian National University, the PAWSEY supercomputing centre located in Western Australia with their Magnus supercomputing clusters, the Queensland Cyber Infrastructure Foundation (QCIF) for the Euramoo supercomputing clusters, the University of Queensland Research Computing Centre (RCC) with their Tinaroo supercomputing clusters, and Goldenorb supercomputing clusters at Australian Institute for Bioengineering and Nanotechnology (AIBN) at the University of Queensland. AFN also acknowledges support from the Australian Government through an Australian Government Research Training Program Scholarship (RTP).

References

[1] Stevens DA, Dahn JR. High capacity anode materials for rechargeable sodium-ion batteries, J Electrochem Soc 147 (2000) 3.
[2] Palomares V, Serras P, Villaluenga I, Hueso KB, Carretero-González J, Rojo T. Na-ion batteries, recent advances and present challenges to become low cost energy storage systems, Energy & Environ Sci 5 (2012) 5884.
[3] Kundu D, Talaie E, Duffort V, Nazar LF. The emerging chemistry of sodium ion batteries for electrochemical energy storage, Angew Chem Int Ed Engl 54 (2015) 3431-3448.
[4] Peng L, Zhu Y, Chen D, Ruoff RS, Yu G. Two-dimensional materials for beyond-lithium-ion batteries, Adv Energy Mater (2016) 1600025.
[5] Balogun MS, Luo Y, Qiu WT, Liu P, Tong YX. A review of carbon materials and their composites with alloy metals for sodium ion battery anodes, Carbon 98 (2016) 162-178.
[6] Luo W, Shen F, Bommier C, Zhu H, Ji X, Hu L. Na-ion battery anodes: Materials and electrochemistry, Acc Chem Res 49 (2016) 231-240.
[7] Lipson AL, Pan BF, Lapidus SH, Liao C, Vaughey JT, Ingram BJ. Rechargeable ca-ion batteries: A new energy storage system, Chem Mater 27 (2015) 8442-8447.
[8] Ponrouch A, Frontera C, Barde F, Palacin MR. Towards a calcium-based rechargeable battery, Nat Mater 15 (2016) 169-172.
[9] Tojo T, Sugiura Y, Inada R, Sakurai Y. Reversible calcium ion batteries using a dehydrated prussian blue analogue cathode, Electrochim Acta 207 (2016) 22-27.

[10] Goriparti S, Miele E, De Angelis F, Di Fabrizio E, Proietti Zaccaria R, Capiglia C. Review on recent progress of nanostructured anode materials for li-ion batteries, J Power Sources 257 (2014) 421-443.
[11] Scrosati B, Garche J. Lithium batteries: Status, prospects and future, J Power Sources 195 (2010) 2419-2430.
[12] Liu YY, Merinov BV, Goddard WA. Origin of low sodium capacity in graphite and generally weak substrate binding of na and mg among alkali and alkaline earth metals, Proc Natl Acad Sci USA 113 (2016) 3735-3739.
[13] Chan KT, Neaton JB, Cohen ML. First-principles study of metal adatom adsorption on graphene, Phys Rev B 77 (2008)
[14] Valencia F, Romero AH, Ancilotto F, Silvestrelli PL. Lithium adsorption on graphite from density functional theory calculations, J Phys Chem B 110 (2006) 14832-14841.
[15] Qie L, Chen W, Xiong X, Hu C, Zou F, Hu P, Huang Y. Sulfur-doped carbon with enlarged interlayer distance as a high-performance anode material for sodium-ion batteries, Adv Sci 2 (2015) 1500195.
[16] Cao Y, Xiao L, Sushko ML, Wang W, Schwenzer B, Xiao J, Nie Z, Saraf LV, Yang Z, Liu J. Sodium ion insertion in hollow carbon nanowires for battery applications, Nano Lett 12 (2012) 3783-3787.
[17] Blackman A, Bottle S, Schmid S, Mocerino M, Wille U. Chemistry. Milton, Qld: John Wiley & Sons Australia; 2012.
[18] Komaba S, Murata W, Ishikawa T, Yabuuchi N, Ozeki T, Nakayama T, Ogata A, Gotoh K, Fujiwara K. Electrochemical na insertion and solid electrolyte interphase for hard-carbon electrodes and application to na-ion batteries, Adv Funct Mater 21 (2011) 3859-3867.
[19] Hahn JR, Kang H, Song S, Jeon IC. Observation of charge enhancement induced by graphite atomic vacancy: A comparative stm and afm study, Phys Rev B 53 (1996) R1725-R1728.
[20] Hashimoto A, Suenaga K, Gloter A, Urita K, Iijima S. Direct evidence for atomic defects in graphene layers, Nature 430 (2004) 870-873.
[21] Carlsson JM, Scheffler M. Structural, electronic, and chemical properties of nanoporous carbon, Phys Rev Lett 96 (2006) 046806-046801.
[22] Lahiri J, Lin Y, Bozkurt P, Oleynik II, Batzill M. An extended defect in graphene as a metallic wire, Nat Nanotechnol 5 (2010) 326-329.
[23] Banhart F, Kotakoski J, Krasheninnikov AV. Structural defects in graphene, ACS Nano 5 (2011) 26-41.
[24] Botello-Mendez AR, Declerck X, Terrones M, Terrones H, Charlier JC. One-dimensional extended lines of divacancy defects in graphene, Nanoscale 3 (2011) 2868-2872.
[25] Wang Y-X, Chou S-L, Liu H-K, Dou S-X. Reduced graphene oxide with superior cycling stability and rate capability for sodium storage, Carbon 57 (2013) 202-208.
[26] Kumar NA, Gaddam RR, Varanasi SR, Yang D, Bhatia SK, Zhao XS. Sodium ion storage in reduced graphene oxide, Electrochim Acta 214 (2016) 319-325.
[27] Erickson K, Erni R, Lee Z, Alem N, Gannett W, Zettl A. Determination of the local chemical structure of graphene oxide and reduced graphene oxide, Adv Mater 22 (2010) 4467-4472.
[28] Bagri A, Mattevi C, Acik M, Chabal YJ, Chhowalla M, Shenoy VB. Structural evolution during the reduction of chemically derived graphene oxide, Nat Chem 2 (2010) 581-587.
[29] Datta D, Li J, Shenoy VB. Defective graphene as a high-capacity anode material for na- and ca-ion batteries, ACS Appl Mater Inter 6 (2014) 1788-1795.
[30] Tsai PC, Chung SC, Lin SK, Yamada A. Ab initio study of sodium intercalation into disordered carbon, J Mater Chem A 3 (2015) 9763-9768.
[31] Yang S, Li S, Tang S, Dong W, Sun W, Shen D, Wang M. Sodium adsorption and intercalation in bilayer graphene from density functional theory calculations, Theor Chem Acc 135 (2016) 1-11.
[32] Okamoto Y. Density functional theory calculations of lithium adsorption and insertion to defect-free and defective graphene, J Phys Chem C 120 (2016) 14009-14014.
[33] Ricco M, Pontiroli D, Mazzani M, Choucair M, Stride JA, Yazyev OV. Muons probe strong hydrogen interactions with defective graphene, Nano Lett 11 (2011) 4919-4922.

[34] Casartelli M, Casolo S, Tantardini GF, Martinazzo R. Spin coupling around a carbon atom vacancy in graphene, Phys Rev B 88 (2013) 195424.
[35] Pontiroli D, Aramini M, Gaboardi M, Mazzani M, Sanna S, Caracciolo F, Carretta P, Cavallari C, Rols S, Tatti R, Aversa L, Verucchi R, Ricco M. Tracking the hydrogen motion in defective graphene, J Phys Chem C 118 (2014) 7110-7116.
[36] Casartelli M, Casolo S, Tantardini GF, Martinazzo R. Structure and stability of hydrogenated carbon atom vacancies in graphene, Carbon 77 (2014) 165-174.
[37] Yoon D, Kim DH, Chung KY, Chang W, Kim SM, Kim J. Hydrogen-enriched porous carbon nanosheets with high sodium storage capacity, Carbon 98 (2016) 213-220.
[38] Dahn JR, Zheng T, Liu Y, Xue JS. Mechanisms for lithium insertion in carbonaceous materials, Science 270 (1995) 590-593.
[39] Stevens DA, Dahn JR. The mechanisms of lithium and sodium insertion in carbon materials, J Electrochem Soc 148 (2001) A803-A811.
[40] Gao W, Alemany LB, Ci LJ, Ajayan PM. New insights into the structure and reduction of graphite oxide, Nature Chemistry 1 (2009) 403-408.
[41] Chen WF, Zhu ZY, Li SR, Chen CH, Yan LF. Efficient preparation of highly hydrogenated graphene and its application as a high-performance anode material for lithium ion batteries, Nanoscale 4 (2012) 2124-2129.
[42] Pramudita JC, Pontiroli D, Magnani G, Gaboardi M, Ricco M, Milanese C, Brand HEA, Sharma N. Graphene and selected derivatives as negative electrodes in sodium- and lithium-ion batteries, ChemElectroChem 2 (2015) 600-610.
[43] Georg Kresse MM, and Jurgen Furthmuller. Vasp user guide [User Guide]Apr 2016.
[44] Blöchl PE. Projector augmented-wave method, Phys Rev B 50 (1994) 17953-17979.
[45] Perdew JP, Burke K, Ernzerhof M. Generalized gradient approximation made simple, Phys Rev Lett 77 (1996) 3865-3868.
[46] Grimme S, Antony J, Ehrlich S, Krieg H. A consistent and accurate ab initio parametrization of density functional dispersion correction (dft-d) for the 94 elements h-pu, J Chem Phys 132 (2010) 154104-154101.
[47] Grimme S, Ehrlich S, Goerigk L. Effect of the damping function in dispersion corrected density functional theory, J Comput Chem 32 (2011) 1456-1465.
[48] Farokh Niaei AH, Hussain T, Hankel M, Searles DJ. Sodium-intercalated bulk graphdiyne as an anode material for rechargeable batteries, J Power Sources 343 (2017) 354-363.
[49] Tang W, Sanville E, Henkelman G. A grid-based bader analysis algorithm without lattice bias, J Phys Condens Matter 21 (2009)
[50] Yu M, Trinkle DR. Accurate and efficient algorithm for bader charge integration, J Chem Phys 134 (2011)
[51] Liang Z, Fan X, Zheng W, Singh DJ. Adsorption and formation of small na clusters on pristine and double-vacancy graphene for anodes of na-ion batteries, ACS Appl Mater Inter 9 (2017) 17076-17084.
[52] Bhauriyal P, Mahata A, Pathak B. Graphene-like carbon–nitride monolayer: A potential anode material for na- and k-ion batteries, J Phys Chem C 122 (2018) 2481-2489.
[53] Mikito K. Stacking-dependent optical absorption in multilayer graphene, New J Phys 15 (2013) 015010.
[54] Garay-Tapia AM, Romero AH, Barone V. Lithium adsorption on graphene: From isolated adatoms to metallic sheets, J Chem Theo Comp 8 (2012) 1064-1071.
[55] Luo G, Zheng Q, Mei W-N, Lu J, Nagase S. Structural, electronic, and optical properties of bulk graphdiyne, J Phys Chem C 117 (2013) 13072-13079.

Supporting Information

Hydrogenated defective graphene as an anode material for sodium and calcium ion batteries: a density functional theory study

Amir H. Farokh Niaei[a], Tanveer Hussain[a], Marlies Hankel[a] and Debra J. Searles[a,b,*]

[a] Centre for Theoretical and Computational Molecular Science, Australian Institute for Bioengineering and Nanotechnology, The University of Queensland, Brisbane, QLD, 4072, Australia

[b]School of Chemistry and Molecular Biosciences, The University of Queensland, Brisbane, QLD, 4072, Australia

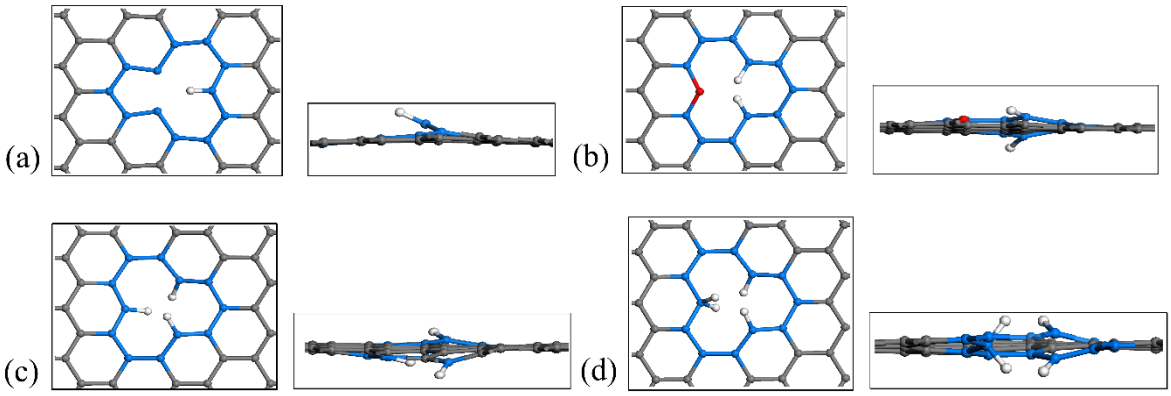

Figure S1. Top and side views of the optimised graphene sheets with hydrogenated MVs. (a) H1-MVG, (b) H2-MVG, (c) H3-MVG, and (d) H4-MVG. Note that the terminology used gives the number of hydrogen atoms after 'H' and the type of vacancy after the underscore. The white atoms are hydrogen atoms and all the others are C atoms. Those coloured in blue surround a vacancy.

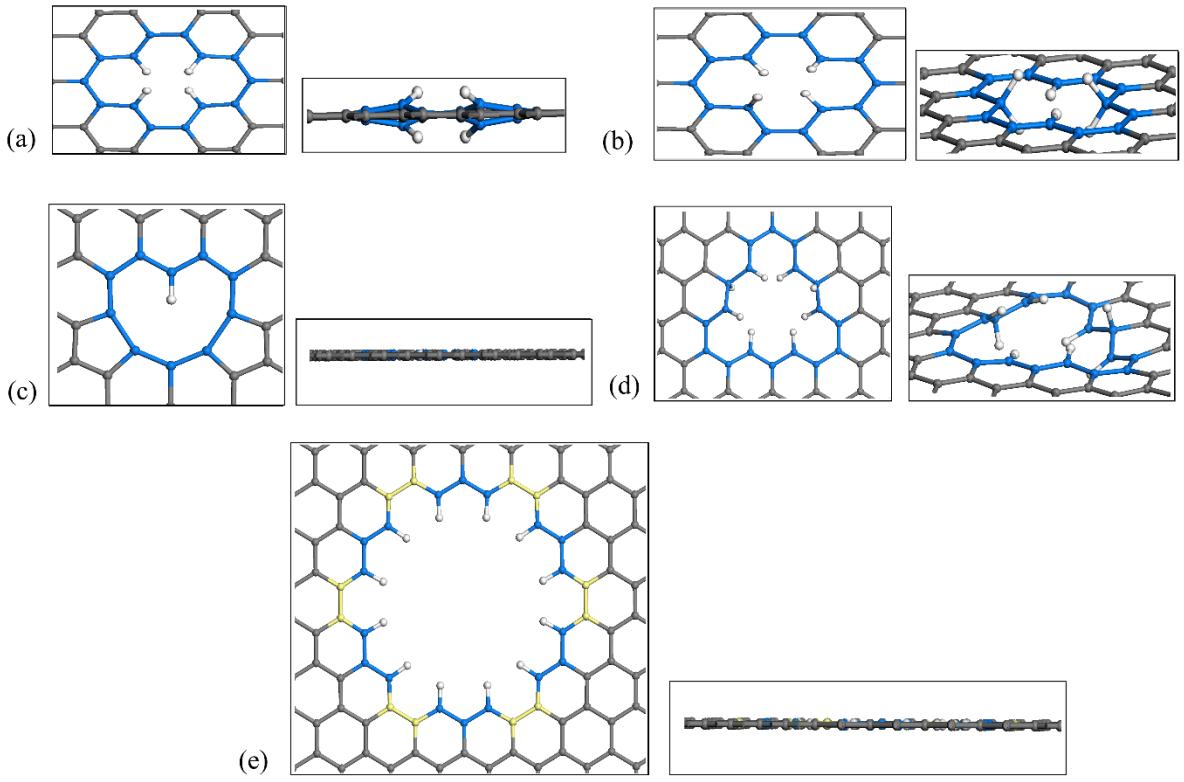

Figure S2. Top and side views of selected graphene materials with hydrogenated vacancies : (a) H4-DVG ($C_{70}H_4$), (b) H6-DVG ($C_{70}H_6$), (c) H1-TVG ($C_{69}H_1$), (d) H8-QVG ($C_{68}H_8$), and (e) H12-24VG ($C_{138}H_{12}$). The white atoms are hydrogen atoms and all others are C atoms. Those coloured in blue surround the vacancy. In e) boat type and zig-zag type carbons around the vacancy are also distinguished by colouring in yellow and blue, respectively.

Table S1. Hydrogenation energy and average C-H bond lengths for graphene sheets with a hydrogenated monovacancy

Material	Empirical formula	Optimal C-H bond configuration	Average C-H bond length / Å	ΔE_H / eV
H1-MVG	$C_{71}H_1$	-	1.08	-4.25
H2-MVG	$C_{71}H_2$	anti	1.09	-3.39
H3-MVG	$C_{71}H_3$	anti	1.07	-3.91
H4-MVG	$C_{71}H_4$	anti	1.08	-2.49

Table S2. Binding energies (eV) of Na at different sites of defective graphene and hydrogenated defective graphene. For location of sites, refer to Figure 4b.

Material	E_b at various sites eV / Na							
	Centre of vacancy	A / B (over vacancy)	C	D	2 Na over	3 Na	4 Na	5 Na
MVG	NS[a]	-2.083	-1.506	-1.320	-1.535	-1.376	-1.228	-1.173
DVG	NS[a]	-1.792	-1.524	-1.282	-1.285	-1.294	-1.256	-1.180
TVG	NS[a]	-2.350	-1.789	-1.581	-1.847	-1.588	-1.470	-1.313
QVG	-0.939	-2.185	-1.886	-1.666	-1.657	-1.480	-1.393	-1.290
24VG	-0.968	-2.909	NS[a]	-1.043	NC[b]	NC[b]	NC[b]	NC[b]
H1-MVG	NS[a]	-1.481	-1.546	-1.363	-1.214	-1.197	-1.111	-1.080
H2-MVG	NS[a]	-2.070	-1.588	-1.458	-1.484	-1.341	-1.279	-1.171
H3-MVG	NS[a]	-1.472	-1.261	-1.162	-1.120	-1.252	-1.069	-1.032
H4-MVG	NS[a]	-0.837	-0.783	-0.764	-1.022	-0.969	NC[b]	NC[b]
H4-DVG	NS[a]	-0.879	-0.878	-0.841	-0.890	-0.998	-0.965	-0.959
H6-DVG	NS[a]	-0.894	-0.888	-0.956	-0.929	-1.056	-1.026	-0.994
H1-TVG	NS[a]	-1.963	-1.773	-1.578	-1.315	-1.295	-1.214	-1.132
H8-QVG	-0.490	-1.241	-1.165	-1.118	NS[a]	NS[a]	DH[c]	DH[c]
H12-24VG	-0.249	-0.842	-0.871	-0.817	NC[b]	NC[b]	NC[b]	NC[b]

[a]NS: not a stable site (movement to another location like the nearest site)

[b]NC: not calculated

[c]DH: detachment of H atoms from substrate after Na adsorption

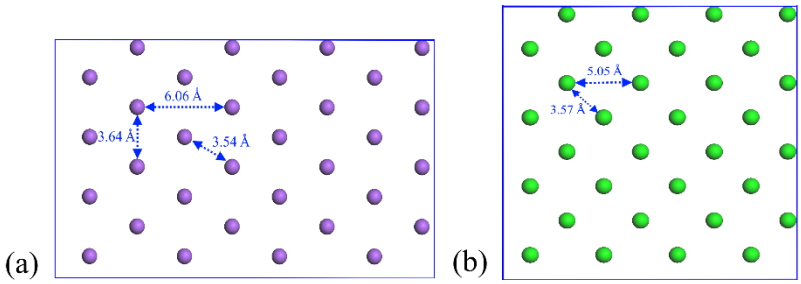

Figure S3. Supercell for a single layer of metal atoms arranged in a (a) (110) configuration for Na (purple), and (b) (100) configuration for Ca (green). These structures were obtained by optimisation using DFT computations, including optimisation of the lattice parameters. The distances between neighbouring atoms are indicated.

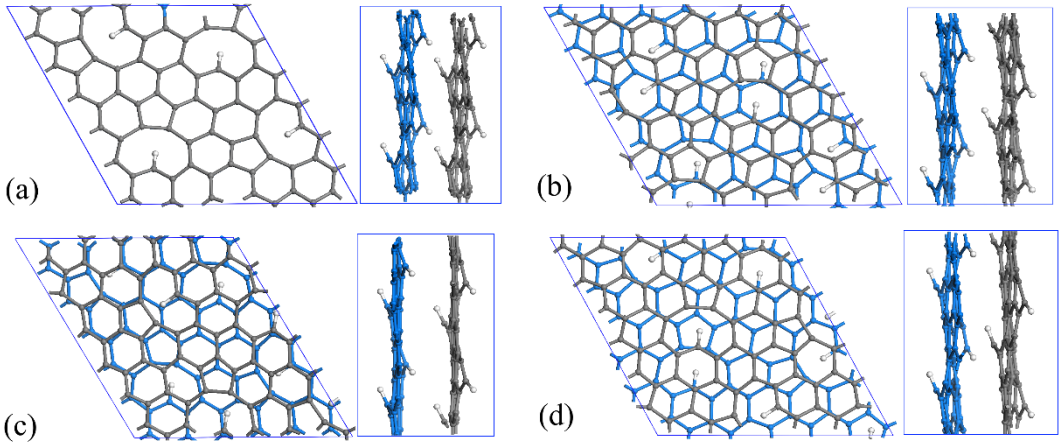

Figure S4. Structures of 4 different stackings of 4(H1-MVG) bulk layered materials with their ΔE (= $E_{ABi\ stacking} - E_{AA\ stacking}$), and inter-layer distances (D). (a) AA stacking with D = 3.49 Å, (b) AB1 stacking with ΔE = +0.9 eV, and D = 3.54 Å, (c) AB2 stacking with ΔE = +1.8 eV and D = 3.80 Å, (d) AB3 stacking with ΔE = +0.9 eV and D = 3.56 Å. The inter-layer distance (D) is measured through vertical distance between the two centres of mass of the two layers. In all the figures, the grey carbon atoms indicate the top layer, and blue carbon atoms indicate the bottom layer. White atoms are hydrogen.

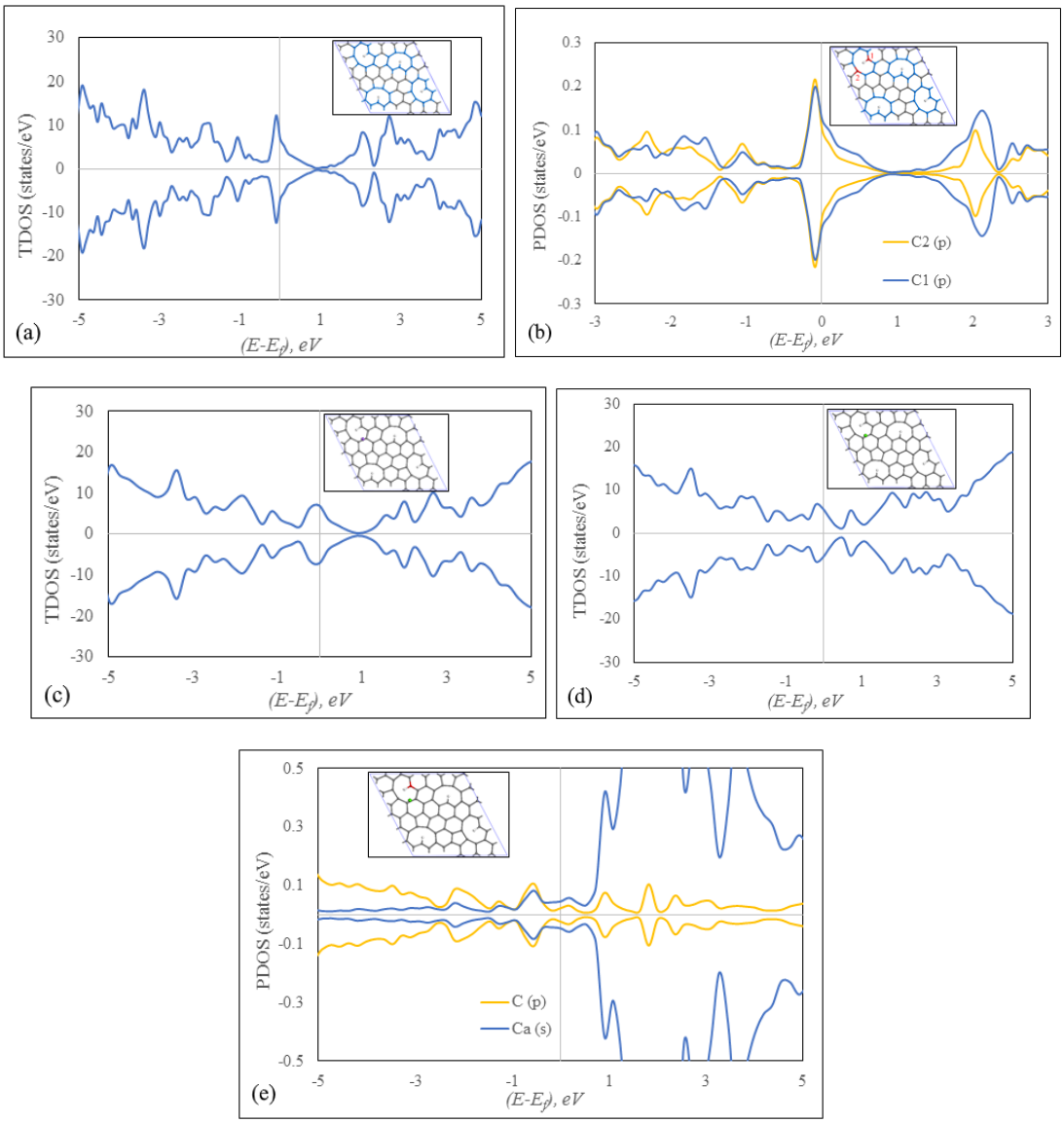

Figure S5. (a) TDOS for 4(H1-MVG) pristine, (b) PDOS for the two indicated carbon atoms in 4(H1-MVG) single layer, (c) TDOS for 1 Na + 4(H1-MVG), (d) TDOS for 1 Ca + 4(H1-MVG), (e) PDOS for 1 Ca and the indicated carbon atom (red).